Lanthanide compounds as catalysts for the one-step synthesis of vinyl chloride from ethylene

Author(s):
Scharfe, Matthias; Lira-Parada, Pedro A.; Amrute, Amol P.; Mitchell, Sharon; Pérez-Ramírez, Javier

Publication date:
2016-12

Permanent link:
https://doi.org/10.3929/ethz-b-000125083

Originally published in:
Journal of Catalysis 344, https://doi.org/10.1016/j.jcat.2016.10.026

Funding acknowledgement:
156107 - Design of oxyhalogenation catalysts for hydrocarbon functionalization (SNF)

Lanthanide compounds as catalysts for the one-step synthesis of vinyl chloride from ethylene

Matthias Scharfe,[†] Pedro A. Lira-Parada,[†] Amol P. Amrute, Sharon Mitchell, and Javier Pérez-Ramírez*

Institute for Chemical and Bioengineering, Department of Chemistry and Applied Biosciences, ETH Zurich, Vladimir-Prelog-Weg 1, 8093 Zurich, Switzerland.

[†] Equal contribution | * Corresponding author. E-mail: jpr@chem.ethz.ch.

Abstract

The industrial manufacture of vinyl chloride relies on a two-step process involving $CuCl_2$-catalyzed ethylene oxychlorination to ethylene dichloride followed by thermal cracking of the latter to vinyl chloride. This work evaluates a wide range of commercial and self-prepared lanthanide (La, Ce, Pr, Nd, Sm, Eu, Gd, Tb, Dy, Ho, and Er) compounds for the one-step production of vinyl chloride from ethylene in a fixed-bed reactor at 623-773 K and 1 bar using feed ratios of C_2H_4:HCl:O_2:Ar:He = 3-6:1-9.6:1-7:3:80-92 and space times of 6-252 g h mol^{-1} (based on ethylene). *Ex situ* characterization by X-ray diffraction, electron microscopy, and X-ray photoelectron spectroscopy reveal that the oxide forms of all compounds, except CeO_2, transform into their respective (oxy)chloride. Among all studied systems, CeO_2 shows the highest activity but suffers from combustion forming CO_x, while europium oxychloride (EuOCl) leads to the best vinyl chloride selectivity of 96% at 20% C_2H_4 conversion for over 100 h on stream. Temperature-programmed reduction with H_2, temperature-programmed desorption of NH_3, and oxidation tests (C_2H_4, CO, and HCl oxidation) unravel the unique balance of mild redox and enhanced acid properties of EuOCl compared to CeO_2, which suppress over-oxidation and boost ethylene dichloride dehydrochlorination. Strategies to couple the excellent selectivity of EuOCl with the high activity of CeO_2 are demonstrated through the synthesis of homogeneous europium-cerium mixed oxides, combining two functions on a single surface. In addition, the engineering of a dual-bed reactor, integrating a CeO_2 bed first to produce ethylene dichloride in high yield which is subsequently transformed to vinyl chloride over EuOCl leads to vinyl chloride yields of up to 30% per pass. These very promising findings constitute a crucial step for process intensification of polyvinyl chloride production and exploring the potential of rare-earth compounds in industrially-relevant reactions.

Keywords: ethylene oxychlorination, lanthanides, europium oxychloride, vinyl chloride monomer, bifunctional catalyst, process intensification

1. Introduction

Polyvinyl chloride (PVC, 44 Mton, annual global growth rate of 3.2%) is an integral part of modern society owing to its widespread applications that improve our everyday life [1,2]. Its monomer, chloroethene (commonly known as vinyl chloride and hereafter denoted as VCM), was first produced on a commercial scale in the 1920s through acetylene hydrochlorination over mercuric chloride catalysts, which still is the main production method in countries such as China, due to cheap availability of coal from which acetylene is produced [3,4]. However, the increasing demand for PVC and rising price of acetylene in the late 1950s prompted a shift in the feedstock to the more economical ethylene in the United States and Europe [3]. Since then, VCM is predominantly produced *via* a two-step process involving the selective oxychlorination of ethene (commonly known as ethylene) to 1,2-dichloroethane (commonly known as ethylene dichloride and hereafter denoted as EDC) over promoted $CuCl_2/\gamma$-Al_2O_3 catalysts in fluidized-bed reactors (T = 473-573 K, P = 1-10 bar) and the subsequent thermal cracking of EDC to VCM (T = 773-873 K, P =25-35 bar) [3,4,5]. The greatest limitations of the current process are the stability issues faced by the copper catalyst, and the limited per pass conversion (50-60% with VCM selectivity > 98%) and high energy demand of the thermal cracking [3]. Despite continued efforts to optimize the robustness of the catalyst by doping with additives such as alkali (Li, Na, K), alkaline earth (Mg, Ca), and rare earth metals (La, Ce), the copper chloride phase is still prone to volatilization and particle agglomeration [6-10]. Besides, the possible intensification of VCM production by integration of the oxychlorination and dehydrochlorination reactions as a one-step process requires a novel catalyst which can combine two functions.

In order to achieve this goal, new materials such as non-halide copper containing catalysts [11] and lanthanide (oxy)chlorides [12], particularly lanthanum oxychlorides, have been reported in the patent literature. However, none of these systems is realized on an industrial scale, most likely due to the low per pass VCM yields and/or stability hurdles faced by these catalysts. Recently, we have uncovered the high stability and remarkable yield of

chlorinated compounds (25% VCM, 25% EDC) over CeO_2. This outstanding performance was attributed to the integration of both redox sites, which catalyze the ethylene oxychlorination to EDC, and acid sites, responsible for the dehydrochlorination of EDC to VCM, on the same catalyst surface.

In spite of these encouraging results, CeO_2 offers significant margins for improvement. In particular, a considerable amount of over-chlorinated compounds (1,2-dichloroethene, commonly known as 1,2-dichloroethylene and hereafter denoted as 1,2-DCE) and combustion products (CO_x) were also formed, decreasing the overall selectivity of EDC and VCM. Moreover, only moderate dehydrochlorination activity was observed. Thus, it can be anticipated that materials exhibiting milder oxidative properties and higher density of strong cites than ceria could lead to enhanced performance. Surprisingly, despite their extensive use as dopants of the $CuCl_2/\gamma$-Al_2O_3 catalysts, lanthanide compounds were never systematically investigated as the main active phase for the conversion of ethylene to VCM. Besides, they were investigated in several other catalyst formulations mainly as dopants and supports [14-18], with the exception of cerium oxide and lanthanum oxide (or (oxy)chloride) which are also studied as the primary catalytic phase in oxidative processes, including CO oxidation [19,20], isobutane oxidation [21], HCl oxidation [22,23], methane oxidative coupling [24], selective reduction of nitrogen oxides [19,25], and methane oxychlorination [26,27].

Herein, the comparison of the performance of a broad set of the most abundant rare-earth compounds leads to the discovery of the exceptional performance of europium oxychloride, exhibiting 96% VCM selectivity at 20% conversion for over 100 h on stream. Structural, redox, and acidic properties are investigated to rationalize the superior performance of europium oxychloride with respect to other lanthanides and parametric studies give insight to the distribution of products. In order to attain superior VCM yields, this novel active phase is combined with the high activity of CeO_2 by synthesis of mixed oxides and through dual-bed reactor concepts. This study comprises the first practically-relevant application of europium in heterogeneous catalysis and the materials presented here have

great potential to be explored in challenging catalyzed reactions, particularly towards the functionalization of hydrocarbons.

2. Experimental methods

2.1. Catalyst preparation

Commercial La_2O_3 (Alfa Aesar, 99.99%), Pr_2O_3 (Alfa Aesar, 99.9%), Nd_2O_3 (Sigma-Aldrich, 99.9%), Sm_2O_3 (Sigma-Aldrich, 99.9%), Eu_2O_3 (Sigma-Aldrich, 99.5%), Gd_2O_3 (Alfa Aesar, 99.99%), Tb_2O_3 (Strem Chemicals, 99.9%), Dy_2O_3 (ABCR, 99.99%), Ho_2O_3 (Fluka Chemie, 99.9%), and Er_2O_3 (Fluka Chemie, 99.9%) were calcined at 773 K, and CeO_2 (Sigma-Aldrich, 99.9%) at 773 K and 1173 K in static air using a heating rate of 5 K min^{-1} and an isothermal step of 5 h prior to their use in catalytic studies. Analysis by X-ray diffraction revealed that the commercial praseodymium oxide actually consisted of Pr_4O_7 and thus it is denoted as such herein. Europium oxide (Eu_2O_3-p-T_{cal}, where T_{cal} denotes the calcination temperature in K), cerium oxide (CeO_2-p-T_{cal}), and mixed europium-cerium oxides ($Eu_xCe_{1-x}O_{2-0.5x}$-cp-T_{cal}, where x represents the molar fraction of Eu in the range of 0.3-0.9) were synthesized by precipitation (p, single oxides) and coprecipitation (cp, mixed oxides) following a protocol reported elsewhere [13]. Briefly, the metal nitrates ($Eu_2(NO_3)_3{\cdot}6H_2O$ (ABCR, 99.9%) for Eu_2O_3-p, $Ce(NO_3)_3{\cdot}6H_2O$ (ABCR, 99.9%) for CeO_2-p, or mixtures for $Eu_xCe_{1-x}O_{2-0.5x}$-cp) were dissolved in deionized water under stirring and H_2O_2 (Acros Organics, 35%) was added to the solution to obtain a molar H_2O_2:M ratio of 3 (M = Eu, Ce, or Eu+Ce). The coprecipitation was achieved by the dropwise addition of aqueous NH_4OH (Sigma-Aldrich, 30%) until a pH of 10.5 was reached. The slurry was stirred for 4 h and washed with deionized water. Upon filtration, the precipitate was dried at 393 K for 12 h and calcined at 773 K for CeO_2-p, 773-1173 K for Eu_2O_3-p, and 773 K for $Eu_xCe_{1-x}O_{2-0.5x}$-cp in flowing air using a heating rate of 5 K min^{-1} and an isothermal step of 5 h.

2.2. Characterization

The metal content was determined by X-ray fluorescence (XRF) spectroscopy using an Orbis PC Micro-EDXRF analyzer with a Rh source (15 kV, 500 μA) and a silicon drift detector. Powder X-ray diffraction (XRD) was measured using a PANalytical X'Pert PRO-MPD diffractometer and Cu-Kα radiation (λ = 0.15418 nm). The data was recorded in the 10-70° 2θ range with an angular step size of 0.017° and a continuing time of 0.26 s per step. N_2 sorption at 77 K was measured in a Quantachrome Quadrasorb-SI analyzer. Prior to the measurements, the samples were outgassed to 50 mbar at 573 K for 3 h. The Brunauer-Emmett-Teller (BET) method [28] was applied to calculate the total surface area, S_{BET}, in $m^2\ g^{-1}$. High-resolution transmission electron microscopy (HRTEM) and elemental mapping using energy-dispersive X-ray spectroscopy (EDX) were conducted on a FEI Talos microscope operated at 200 kV. All samples were dispersed as dry powders onto lacey carbon coated nickel or molybdenum grids. X-ray photoelectron spectroscopy (XPS) measurements were performed on a Physical Electronics Quantum 2000 X-ray photoelectron spectrometer using monochromatic Al-Kα radiation generated from an electron beam operated at 15 kV, and equipped with a hemispherical capacitor electron-energy analyzer. The powdered sample was firmly pressed onto the foil. The area analyzed was 150 μm in diameter and the electron take-off angle was 45°. The pass energy used for the detailed spectra of the C 1*s*, O 1*s*, Cl 2*p*, Eu 3*d*, Eu 4*d*, and Ce 3*d* core levels was 46.95 eV to yield a total analyzer energy resolution of 0.95 eV. The spectrometer energy scale was calibrated for the Au 4*f* electrons to be at 84.0±0.1 eV. Partial compensation of surface charging during spectra acquisition was obtained by the simultaneous operation of electron and argon ion neutralizers. Elemental concentrations are given in atomic percent using the measured photoelectron peak areas after Shirley background subtraction and the built-in sensitivity factors for calculation. Temperature-programmed desorption of ammonia (NH_3-TPD) and temperature-programmed reduction with hydrogen (H_2-TPR) were performed using a Micromeritics Autochem II 2920 unit equipped with a thermal conductivity detector

coupled to a MKS Cirrus 2 mass spectrometer. The powder sample (0.1 g) was loaded into a U-shaped quartz micro-reactor, pretreated in He (20 cm^3 STP min^{-1}) at 573 K for 3 h, and cooled to 373 K in He. For NH_3-TPD experiments, ammonia was chemisorbed at 473 K in three consecutive cycles of saturation with 5 vol.% NH_3/He (20 cm^3 STP min^{-1}) for 30 min followed by purging with He (20 cm^3 STP min^{-1}) at the same temperature for 30 min. Desorption of NH_3 was monitored in the range of 473-1273 K using a heating rate of 20 K min^{-1} and a He flow of 20 cm^3 STP min^{-1}. For H_2-TPR experiments, the sample was pretreated in He (20 cm^3 STP min^{-1}) at 423 K for 1 h, and cooled to room temperature followed by ramping the temperature at 10 K min^{-1} up to 1273 K in 5 vol.% H_2 (20 cm^3 STP min^{-1}).

2.3. Catalytic tests

The gas-phase oxychlorination of ethylene was investigated at ambient pressure in a continuous-flow fixed-bed reactor (**Scheme 1**). The set-up consists of (*i*) mass flow controllers to feed C_2H_4 (PanGas, 20.15% in He), HCl (Air Liquide, purity 2.8, anhydrous), O_2 (Messer, 10.06% in He), He (PanGas, purity 5.0) as a carrier gas, and Ar (PanGas, purity 5.0) as an internal standard, (*ii*) a syringe pump (Nexus 6000, Chemyx) to feed EDC (Fluka, 99.5%), (*iii*) a vaporizer operated at 403 K accommodating a quartz T-connector filled with glass beads to vaporize EDC, (*iv*) an electrically heated oven hosting a quartz micro-reactor equipped with a K-type thermocouple whose tip reaches the center of the catalyst bed, (*v*) downstream heat tracing to avoid any condensation of the reactants and products, and (*vi*) a gas chromatograph coupled to a mass spectrometer (GC-MS) for on-line analysis. The effluent stream was neutralized by passing it through an impinging bottle containing an aqueous NaOH solution (1 M). The catalyst (W_{cat} = 0.25-2 g, particle size, d_p = 0.4-0.6 mm) was loaded in the micro-reactor (10 mm inner diameter) and pretreated in He at 473 K for 30 min. Thereafter, a total flow (F_T) of 100 cm^3 STP min^{-1} containing 3-6 vol.% C_2H_4, 1-9.6 vol.% HCl, 1-7 vol.% O_2, and 3 vol.% Ar as internal standard, balanced in He was fed to

the reactor at a bed temperature (T) of 623-773 K and pressure (P) of 1 bar. Note that relatively low feed concentrations were selected to prevent corrosion, enable safe handling, and minimize the formation of hot spots in the catalyst bed due to the high reaction exothermicity. Temperature measurements in a reference experiment on CeO_2-1173 (at 31% C_2H_4 conversion), evidenced a temperature gradient of 0.9 K across the bed when the temperature in the center of the catalyst bed was set to 673 K (**Scheme 1**). The standard conditions of 3 vol.% C_2H_4, 4.8 vol.% HCl, and 3 vol.% O_2 were chosen based on the literature [8,13]. The space time, defined as the ratio of the catalyst mass and the inlet molar flow of ethylene as the limiting reactant, $W_{cat}/\dot{n}^0(C_2H_4$ was varied in the range of 6-252 g h mol^{-1}. In the dehydrochlorination tests, 1.5 vol.% EDC was fed to the catalyst (W_{cat} = 0.5 g, d_p = 0.4-0.6 mm) using He as carrier gas (F_T = 100 cm^3 STP min^{-1}) with or without addition of HCl (4.8 vol.%) and O_2 (3 vol.%) at T = 523-773 K and $W_{cat}/\dot{n}^0$(EDC) = 126 g h mol^{-1}. Prior to the analysis of the reaction mixtures, the catalysts were equilibrated for at least 1 h under each condition. The gas composition at the reactor outlet containing reactants (C_2H_4, O_2, HCl) and products (EDC, VCM, 1,2-DCE, CO, CO_2) was analyzed online using a gas chromatograph equipped with a GS-CarbonPLOT column coupled to a mass spectrometer (Agilent GC 7890B, Agilent MSD 5977A) with a triple-axis detector and an electron multiplier. A representative chromatogram is depicted as an inset in **Scheme 1**. In the oxidation tests, C_2H_4 (3 vol.%), CO (2.5 vol.%), or HCl (3 vol.%) and O_2 were fed in a 1:1 volumetric ratio. In the HCl oxidation tests, the Cl_2 production was quantified by offline iodometric titration (using a Mettler Toledo G20 Compact Titrator) of triiodide, formed by purging the Cl_2 containing reactor outlet through an aqueous KI (Sigma-Aldrich, 99.5%) solution (0.1 M), with 0.01 M sodium thiosulfate solution (Sigma-Aldrich, 99.99%). The conversion of HCl, X(HCl), was calculated using **Eq. 1**,

$$X(\mathrm{HCl}) = \frac{2x_{\mathrm{Cl_2,outlet}}}{x_{\mathrm{HCl,inlet}}} \cdot 100, \% \qquad \text{(Eq. 1)}$$

where $x_{HCl,inlet}$ and $x_{Cl_2,outlet}$ denote the volumetric concentration of HCl and Cl_2 at the reactor inlet and outlet, respectively. The conversion of carbon containing reactant, $X(i)$, where i denotes C_2H_4 or CO, was calculated according to **Eq. 2**,

$$X(i) = \frac{x_{i,inlet} - x_{i,outlet}}{x_{i,inlet}} \cdot 100, \% \quad \text{(Eq. 2)}$$

where $x_{i,inlet}$ and $x_{i,outlet}$ denote the volumetric concentration of i at the reactor inlet and outlet, respectively. The selectivity and yield of a reaction product j, $S(j)$ and $Y(j)$, were calculated according to **Eqs. 3 and 4**,

$$S(j) = \frac{x_j / v_j}{\sum x_j / v_j} \cdot 100, \% \quad \text{(Eq. 3)}$$

$$Y(j) = \frac{X(i) \cdot S(j)}{100}, \% \quad \text{(Eq. 4)}$$

where x_j and v_j denote the volumetric concentrations of product j at the reactor outlet and the corresponding stoichiometric factor with respect to the number of carbon atoms, respectively (*e.g.*, $C_2H_4 + 2O_2 \rightarrow 2CO + 2H_2O$, $v_{CO} = 2$). The rate of VCM production, r(VCM), and the rate of ethylene consumption, $r(C_2H_4)$ were calculated using **Eq. 5 and 6**,

$$r(\text{VCM}) = \frac{x_{C_2H_4,inlet} \cdot F_T \cdot X(C_2H_4)/100 \cdot P \cdot S(\text{VCM})/100}{R \cdot T_{STP} \cdot W_{cat} \cdot S_{BET}}, \text{mol h}^{-1}\,\text{m}^{-2} \quad \text{(Eq. 5)}$$

$$r(C_2H_4) = \frac{x_{C_2H_4,inlet} \cdot F_T \cdot X(C_2H_4)/100 \cdot P}{R \cdot T_{STP} \cdot W_{cat} \cdot S_{BET}}, \text{mol h}^{-1}\,\text{m}^{-2} \quad \text{(Eq. 6)}$$

where $x_{C_2H_4,inlet}$, R, and T_{STP}, denote volumetric reactor inlet C_2H_4 concentration, gas constant, and temperature at standard conditions, catalyst mass, and specific surface area, respectively. The carbon mass balance error ε_C was determined using **Eq. 7**,

$$\varepsilon_C = \left| \frac{\sum x_{i,j,inlet} / v_{i,j,inlet} - \sum x_{i,j,outlet} / v_{i,j,outlet}}{\sum x_{i,j,inlet} / v_{i,j,inlet}} \right| \cdot 100, \% \quad \text{(Eq. 7)}$$

where $x_{i,j}$ and $v_{i,j}$ denote the concentration of reactant i or product j at the reactor inlet or outlet and the corresponding stoichiometric factor with respect to the number of carbon atoms, respectively. Each catalytic data point reported is an average of at least three measurements. The carbon mass balance in all catalytic tests closed at 96% or higher. After the tests, the catalyst bed was quenched to room temperature in He flow.

3. Results and discussion

3.1. Performance of lanthanide compounds in ethylene oxychlorination

The lanthanide oxides evaluated in this study were characterized by XRF (**Fig. S1**) and XRD (**Fig. S2**) to confirm their compositional and phase purity. All results coincided with the manufacturers specifications except in the case of praseodymium, which was found to be present mainly in the form of Pr_4O_7 rather than Pr_2O_3. Besides, the post-reaction structural analysis revealed that all samples except CeO_2 undergo phase transitions to their respective (oxy)chloride phase (*vide infra*; *e.g*. Eu_2O_3 transforms to EuOCl). For this reason, the catalysts are denoted according to the crystalline phase evidenced by XRD in the equilibrated materials (after treatment for at least 1 h under reaction conditions).

Comparative assessment in ethylene oxychlorination (**Fig. 1**), revealed that the rare earth materials can be classified into three groups according to their performance. The first (SmOCl, $ErCl_3$, TbOCl, and HoOCl) and second (PrOCl, DyOCl, GdOCl, $NdCl_3$, $LaCl_3$) both display only minor activity, and are differentiated by the observation of chlorinated products (EDC or VCM) which are only formed over the latter group. In contrast, the third group, comprising CeO_2 and EuOCl, stands out, exhibiting notably higher C_2H_4 conversion and selectivity to chlorinated products than either of the other groups. CeO_2, which was previously studied in this reaction, demonstrated the highest yield of chlorinated compounds. On the other hand, EuOCl interestingly showed the highest selectivity to VCM (51% *versus* 30% over CeO_2 at 12 and 26% C_2H_4 conversion, respectively) and no formation of CO_2. Two advantageous features of EuOCl can be highlighted: the suppressed CO_2 formation indicates an inherently lower reducibility of EuOCl with respect to CeO_2 while still maintaining the ability to form EDC and the low EDC selectivity over EuOCl evidences that more than 90% of the EDC formed is directly transformed to VCM. In addition, EuOCl shows a 1.5 fold higher relative ethylene conversion per unit surface area of the equilibrated sample as determined by N_2 sorption (**Table 1**) than CeO_2. In fact, comparison of the surface

normalized rate of VCM production as a function of the inverse of temperature (**Fig. 1**, inset) reveals that EuOCl outperforms CeO_2 in the whole temperature range.

Previously [13], we showed that the ethylene oxychlorination performance of CeO_2 could be enhanced through the preparation of materials with higher surface areas by precipitation. Following this strategy, a series of europium-based catalysts (EuOCl-p-T_{cal}, where T_{cal} denotes the calcination temperature) were prepared with surface areas comparable to that of CeO_2. Surprisingly, however, these samples did not lead to the expected increase in conversion, but completely suppressed the oxidation reaction to CO and largely increased the yields of EDC and VCM (**Fig. 1**), which were highest over EuOCl-p-973. In this case, EuOCl-p-973 was found to be one order of magnitude more reactive than CeO_2 and comparable to EuOCl in terms of surface normalized rate (**Fig. 1**, inset).

3.2. Catalyst evolution in ethylene oxychlorination

Analysis of the structure, composition, porosity, and surface properties of the equilibrated catalysts provides insight into the trends observed during the comparative evaluation in ethylene oxychlorination. As mentioned (*vide supra*), phase transformations were observed in all of the catalysts after evaluation in the ethylene oxychlorination reaction, except CeO_2. Nonetheless, this phase evolution should be regarded as an equilibration step leading to the successful formation of the active (oxy)chloride phase rather than proof of instability. In fact, no catalyst volatilization was evidenced. Comparison by XRD (**Figs. 2**, **S2**) identifies three different degrees of transformation, encompassing the preservation of the bulk oxide (CeO_2) [13,22], the formation of an oxychloride (SmOCl, TbOCl, HoOCl, PrOCl, EuOCl), and the complete transformation to the chloride phase ($ErCl_3$, $NdCl_3$, $LaCl_3$). Despite exhibiting distinct performance, only a single europium oxychloride phase is observed in EuOCl-p-973 and EuOCl. Slightly sharper reflections in the latter reflect increased average particle size, which is in line with lower surface area. A Scherrer-based analysis confirms an average crystal size of 31 nm for EuOCl in comparison with 13 nm for the EuOCl-p-973 sample.

Examination of $LaCl_3$, EuOCl, and CeO_2 by TEM and elemental mapping clearly revealed the different extent of chlorination in these samples. $LaCl_3$ (**Fig. 3a**), which fully chlorinates upon equilibration under ethylene oxychlorination conditions, comprises large agglomerates of between 100-200 nm diameter. The relative intensity of the Cl and La lines in the EDX spectrum of *ca*. 3 agrees well with the stoichiometry of the metal chloride. Comparatively, EuOCl as well as EuOCl-p-973 (**Fig. 3b**,**c**) features much smaller particles of *ca*. 40 nm in diameter and a Cl:Eu intensity ratio close to unity, as expected from a pure oxychloride phase. In both cases, no considerable change in crystal size is observed between the as prepared and equilibrated materials. Finally, CeO_2 evidences even smaller nanoparticles of 10-20 nm (as prepared: 5-10 nm) in diameter and exhibits only a minor chlorine peak in the EDX spectrum (**Fig. 3d**, inset), consistent with the low intensity of this element in the corresponding map and the preservation of the oxide phase evidenced by XRD. To detect possible differences in the surface and bulk composition, XPS analysis was conducted for the as-prepared Eu_2O_3-p-973, which evidences a Eu 4*d* core level band structure composed of the Eu $4d_{3/2}$ and Eu $4d_{5/2}$ peaks, characteristic of Eu_2O_3 (**Fig. 4a**) [29,30]. Upon use in ethylene oxychlorination, both of these peaks were shifted to higher binding energy by 2 eV, pointing to the presence of neighboring atoms of high electronegativity [29]. A signal detected in the survey spectrum at 198.5 eV [31] in the Cl 2*p* region unequivocally confirmed the presence of chlorine at the surface (**Fig. 4b**). In fact, the surface atomic concentrations of Eu, O, and Cl were determined to be 33, 36, and 30%, respectively, which is close to the stoichiometry of the oxychloride phase.

Overall, these results demonstrate that ethylene oxychlorination over the lanthanide compounds studied is essentially catalyzed by the oxychloride or chloride phase, including in the case of CeO_2 in which chloride species exist at the surface. However, there are no detectable structural differences between EuOCl and EuOCl-p-973 that would explain their disparity in selectivity. As on CeO_2 the suppression of combustion and the formation of VCM were linked to moderated oxidative properties (catalyzing ethylene oxychlorination to EDC)

and the presence of acid sites (needed for EDC dehydrochlorination to VCM [32]), the properties of EuOCl-p-973 and CeO_2 were investigated by H_2-TPR and NH_3-TPD. PrOCl was also studied as a moderately active and unselective reference.

The H_2-TPR profile of CeO_2 **(Fig. 5a)** shows two H_2 consumption peaks at 761 and 1090 K, which are attributed to the reduction of labile surface or near-surface oxygen species and the bulk, respectively [32,34]. This very much resembles the analysis of the as-prepared CeO_2 samples [22] and indicates that the reducibility of this oxide is not significantly altered under reaction conditions. Pr_4O_7 displays a H_2 consumption peak centered at 978 K, however, no H_2 consumption is observed for its analogue PrOCl, indicating that the oxychloride is irreducible in this temperature range. This explains the negligible yields of VCM and CO, observed over this catalyst, which are comparable to the inactive materials. Eu_2O_3-p-973 evidences a broad H_2 consumption peak in the range of 882-1197 K, while EuOCl-p-973 shows H_2 consumption at significantly higher temperature (similar trend for Eu_2O_3 and EuOCl). Thus, the diminished reducibility of europium oxychlorides compared to CeO_2 is responsible for the lower activity and most importantly the suppression of combustion. However, it is still sufficient to catalyze the formation of EDC.

NH_3-TPD analyses confirmed that the equilibrated CeO_2 and EuOCl-p-973 catalysts both exhibit significant NH_3 desorption in the range of 525-775 K (**Fig. 5b**), evidencing the presence of acid sites. This is in line with previous studies on CeO_2 after treatment under chlorination conditions [13,35]. The lower acidity of EuOCl with respect to EuOCl-p-973 is also in accordance with the lower VCM selectivity of the former. Surprisingly, PrOCl shows the highest amount of acid sites by far, which causes the complete transformation of any EDC produced to VCM. Quantification of the amount of ammonia evolved from the two materials with highest VCM yields reveals a significantly higher acid site density in EuOCl-p-973 (1.92 $\mu mol\ g^{-1}$) than CeO_2 (1.45 $\mu mol\ g^{-1}$), explaining the enhanced VCM formation over the former.

3.3. Influence of operating conditions

In view of the unprecedented selectivity of EuOCl-p-973, the impact of reaction conditions (namely temperature, HCl and O_2 feed contents, and contact time) on the conversion and product distribution was studied (**Fig. 6**). These results are compared with CeO_2 calcined at 1173 K (CeO_2-1173), which was previously reported in ethylene oxychlorination [13]. Both catalysts exhibit an increased conversion with temperature (**Fig. 6a**), but the enhancement is lower over EuOCl-p-973 than CeO_2-1173. Accordingly, the apparent activation energy (determined from Arrhenius plots, **Fig. S3**) is slightly higher for CeO_2-1173 (28 kJ mol^{-1}) than for EuOCl-p-973 (17 kJ mol^{-1}). Considering the product distribution, the selectivity to VCM increases with reaction temperature over both catalysts, which correlates with a parallel decrease in the EDC selectivity. No CO_x formation is evidenced over EuOCl-p-973 up to 773 K at which point a minor amount of CO is observed, whereas CeO_2-1173 suffers from over-oxidation above 673 K, leading to *ca*. 50% selectivity to CO_x (at 50% C_2H_4 conversion) at 773 K. However, in this comparison of the effect of temperature on the selectivity patterns of the catalysts, the conversion levels differ due to the stronger activity dependence on temperature of CeO_2 than that of EuOCl. Therefore, to decouple the effect of temperature and conversion, the latter was raised by changing the space time at 723 K over both catalysts (**Fig. 6d**). Upon increasing the C_2H_4 conversion over EuOCl-p-973, the selectivity to VCM strongly increases and, reaching 100% at 25% conversion. The selectivity to EDC decreases in equal order, which is consistent with the successive transformation of ethylene to EDC and its dehydrochlorination to VCM. A qualitatively similar decrease of EDC selectivity is also observed over CeO_2-1173 at comparable conversion levels. Nonetheless, the formation of combustion (CO_x) and over-chlorinated (1,2-DCE) products is enhanced instead of VCM.

Varying the feed composition also highlights significant differences in the behavior of the two catalysts. Neither the conversion nor the product distribution is significantly affected by the HCl or O_2 feed contents within the investigated range (*i.e*. zero order with respect to HCl

and O_2) over EuOCl-p-973. In contrast, CeO_2-1173 exhibits a positive linear activity trend with the HCl feed content and a second order dependency with respect to oxygen (**Fig. 6b**,**c**). Furthermore, the EDC selectivity increases with the HCl content in the feed over CeO_2-1173, compensated by decreased CO_x formation. This is expected as a higher degree of chlorination lowers the oxidative strength of the CeO_2-1173 surface [13,22] and provides more available sites for chlorination. The inverse argument applies for raising the oxygen content, which favors combustion and lowers the selectivity to EDC linearly by decreasing the degree of surface chlorination [22]. Combining these results with the insights gained from the bulk and surface characterization, important differences between the two materials can be pointed out. Although CeO_2-1173 preserves the bulk structure of the oxide, the reaction environment alters the nature of the surface from a more oxide- to a more chloride-dominated structure, which have different oxidative properties. In contrast, once formed the surface structure of EuOCl-p-973 remains unaltered by the feed conditions. Thus, a change in reaction atmosphere only affects the thermodynamic equilibria, but not the nature of redox sites.

To further understand the selectivity patterns of catalysts in ethylene oxychlorination, the reaction was split into the four possible processes that can impact the VCM formation. These include the oxidation of C_2H_4 to CO_x, CO to CO_2, and HCl to Cl_2, as well as the dehydrochlorination of EDC to VCM (**Fig. 7**). Each reaction was performed over equilibrated samples: CeO_2 (exhibiting the highest activity), EuOCl-p-973 (attaining the highest VCM yield), and PrOCl (representative of samples exhibiting low activity and high CO formation). In C_2H_4 and HCl oxidation reactions, CeO_2 is the most active material, especially at higher temperatures (**Fig. 7a**,**b**), which correlates with its higher reducibility (*vide supra*, **Fig. 5a**). PrOCl also shows activity for the oxidation of C_2H_4 and CO, with similar or lower light-off temperatures compared to CeO_2, respectively. Note that no CO_2 was generated on PrOCl during ethylene oxychlorination, while in separate oxidation experiments it converted both C_2H_4 and CO to CO_2. XRD analysis revealed that the PrOCl phase partially decomposes and

re-transforms to the Pr_4O_7 phase during oxidation reactions in the absence of HCl, which is again reducible (**Figs. 5a**, **S4a**,**b**) and thus causes the formation of CO_x. The limited yield of chlorinated products formed on PrOCl (**Fig. 1**) is explained by its inability to release chlorine as seen from its negligible activity in HCl oxidation tests (**Fig. 7c**). In stark contrast to the above-mentioned systems, EuOCl-p-973 is essentially inactive for the C_2H_4 and CO oxidation reactions (**Fig. 7a**,**b**), preserves the EuOCl phase under oxidizing conditions (**Fig. S4**), and has moderate ability to transfer chlorine as evidenced by its mild HCl oxidation activity above 673 K (**Fig. 7c**). Thus, it appears that the stability of the oxychloride phase and the ability to release chlorine from the surface are key to suppressing the formation of undesired oxidation products and to chlorinate ethylene.

Finally, the dehydrochlorination of EDC to VCM, was investigated by feeding 1.5 vol.% EDC without or with addition of 3 vol.% O_2 and 4.8 vol.% HCl to the feed (**Fig. 7d**). The EDC concentration was selected to simulate a 50% ethylene conversion to EDC. Furthermore, since CeO_2 was known to yield a 90% conversion to VCM in mixed EDC:O_2:HCl feeds [13], a high EDC feed concentration was preferred to provide improved sensitivity to differences in the performance. Dehydrochlorination activity was observed in all cases. This differed from our previous study, in which CeO_2 was found to be inactive in a pure EDC feed. The latter finding can be explained by the fact that in the present study, we evaluated the dehydrochlorination performance on catalysts equilibrated in ethylene oxychlorination, which increased the acidity of these samples. Albeit demonstrating a limited selectivity to chlorinated products in ethylene oxychlorination, PrOCl displays the best EDC dehydrochlorination performance, with or without cofeeding oxygen and HCl, which can be linked to the highest density of acid sites evidenced in this material. However, the inferior performance of PrOCl in ethylene oxychlorination can be related to the low tendency of this catalyst to release chloride and it negligible reducibility (*vide supra*). CeO_2 demonstrates a linear dehydrochlorination trend with temperature when only EDC is fed, while an increased VCM yield and a shift to lower temperatures is attained when O_2 and HCl are mixed with the

EDC. Nevertheless, at 773 K the yield is heavily decreased due to more extensive CO formation, which can be traced back to the higher reducibility of CeO_2 (**Figs. 5a, 7a**,**b**) that causes the combustion of chlorinated products. EuOCl-p-973 exhibits a linear trend with no CO_x formation and an enhanced selectivity to VCM when $HCl+O_2$ is added to the feed.

3.4. Integration of high activity and selectivity functions

The fact that the VCM yield over EuOCl is limited by its low intrinsic oxychlorination activity while the VCM selectivity over CeO_2 is compromised by the formation of CO_x and over-chlorinated compounds, encouraged us to consider the possibility of integrating the advantageous qualities of each of these rare-earth compounds in the form of mixed oxides. Consequently, we prepared samples with molar fractions of europium ranging from 0.3-0.9 by coprecipitation (**Table 2**). The resulting materials were evaluated in ethylene oxychlorination at 673 K to maximize the activity while minimizing the likelihood of over-oxidation (**Fig. 8**). The yield of chlorinated products (and thus the C_2H_4 conversion) is found to reach a maximum over $Eu_{0.4}Ce_{0.6}O_{1.8}$-cp-773. A further increase in cerium contents in these precipitated samples cause a drop in activity and also lead to the formation of over-chlorinated products (1,2-DCE).

Analysis by N_2 sorption indicated that the total surface area of the mixed oxides was generally lower than the corresponding single phases (**Table 2**), which gives a first hint of the interaction of Eu and Ce in these systems. Due to the similar crystal structures of Eu_2O_3 and CeO_2, it is difficult to conclude whether the fresh $Eu_xCe_{1-x}O_{2-0.5x}$-cp-T_{cal} materials are physical mixtures of the single oxides or atomically-dispersed mixed metal oxides (*i.e.* having metal to metal interactions/bonding within the oxide network) by XRD (**Fig. S5**). Analysis of the equilibrated samples only evidences the presence of the EuOCl phase in samples with a europium fraction above 0.6. The fact that the oxychloride is not observed for $x \leq 0.5$ corroborates the strong interaction between Eu and Ce in the mixed phase. Consistently, the cell parameter of 5.38 Å was derived for $Eu_{0.4}Ce_{0.6}O_{1.8}$-cp-773, the best

sample in terms of VCM yield, which lies between that of the CeO_2-p-773 (5.35 Å) and Eu_2O_3-p-773 (5.41 Å). Examination by electron microscopy (**Fig. 3e**) shows that the equilibrated sample is composed of small nanoparticles of *ca*. 5-10 nm, preserving the crystallinity of the as prepared material (not shown for brevity). The elemental map reveals a very homogeneous distribution of europium and cerium atoms, which is also similar to the fresh analogue. Interestingly, the EDX spectrum evidences a small amount of chlorine in the equilibrated sample, which is also corroborated by XPS results showing a shift of the Eu $4d_{3/2}$ and Eu $4d_{5/2}$ peaks to higher binding energy compared to the as-prepared sample due to the presence of chlorine (**Fig. 4b**). Thus, the oxychloride phase could still exist at the surface leading to high acidity. This reasoning is consistent with the highest VCM yield of this sample (**Fig. 1**). Comparing the performance of $Eu_{0.4}Ce_{0.6}O_{1.8}$-cp-773 with EuOCl-p-973 and CeO_2-p-773, it is clear that the mixed oxide leads to very selective VCM formation (**Fig. 8**) and minimal combustion.

Since stability is a crucial driver in the hunt for new catalytic systems to improve the current ethylene oxychlorination process, the long-term performance of EuOCl-p-973 and $Eu_{0.4}Ce_{0.6}O_{1.8}$-cp-773 was evaluated, demonstrating a stable operation in ethylene oxychlorination for over 100 and 40 h on stream with VCM yields of 15% and 19%, respectively (**Fig. 9**). Even though a minor amount of 1,2-DCE (estimated by carbon mass balance error of about 5-6%) is observed for $Eu_{0.4}Ce_{0.6}O_{1.8}$-cp-773 up to 20 h, after which it drops with time-on-stream, the mixed oxide evidences higher activity as it is operated at 50 K lower temperature and one fourth of the space time (63 g h mol^{-1} compared to 252 g h mol^{-1}). To further assess the stability of EuOCl, we conducted a catalytic test doubling the reactant concentration, which resulted in a very similar selectivity pattern (4% EDC, 96% VCM) as observed under standard conditions at comparable C_2H_4 conversion (19%). Besides, no volatilization of the active phase was evidenced, for example by deposits commonly observed on the reactor walls when using unstable materials, under either condition. Still, the VCM yield achieved is not yet optimal (**Fig. 8**). In fact, although CeO_2-p-

773 suffers from CO_x and 1,2-DCE formation, the overall yield of desired EDC and VCM was higher compared to $Eu_{0.4}Ce_{0.6}O_{1.8}$-cp-773.

As an alternative approach to improve the VCM yield, CeO_2 and EuOCl were united in a dual-bed reactor, combining the high activity of CeO_2 in a first bed in the direction of flow in order to enhance the EDC formation with the unique selectivity to VCM of EuOCl due to its acidity in a second bed (CeO_2-p-EuOCl-p-db). Advantageously, this could also enable an efficient utilization of the heat generated by the exothermic oxychlorination in the downstream endothermic dehydrochlorination. This system indeed results in the highest VCM (27%) and VCM+EDC (33%) yields observed so far at the standard space time of 63 g h mol^{-1} applied in this study. Even though small amounts of side products (CO_2 and 1,2-DCE) are formed in the first bed by CeO_2 (**Fig. 8**), this dual-bed system shows the highest rate of VCM production per unit surface area of the catalyst (**Table 2**). Since both, EuOCl (**Fig. 9**) and CeO_2 [13] are individually stable, a highly robust operation of this dual-bed reactor can be anticipated.

4. Conclusions

In this study, we developed a fundamental understanding of the ethylene oxychlorination chemistry on scarcely studied rare-earth compounds. Through the integration of steady-state catalytic tests and advanced characterization, we identified EuOCl as the best catalyst for direct VCM production, leading to 96% selectivity and no CO_x formation at 20% ethylene conversion for over 100 h on stream. The consecutive conversion of ethylene to EDC and EDC to VCM confirmed the bifunctional reaction mechanism over this catalyst. This unique behavior was found to originate from the transformation of the initial Eu_2O_3 phase to a stable oxychloride. The latter was completely inert towards ethylene and CO oxidation, which explains the absence of undesired CO_x, while it exhibited moderate HCl oxidation, demonstrating its ability to chlorinate ethylene. Other lanthanide oxides, except CeO_2 which retained the oxide structure after reaction, also transformed to their respective oxychloride or

chloride phases. However, these oxychlorides were either essentially inactive in ethylene oxychlorination or decomposed in oxidative conditions and catalyzed undesired oxidations forming significant amounts of CO_x, as demonstrated for the case of PrOCl. Another crucial aspect of the EuOCl phase was the presence of a high concentration of acid sites, which catalyzed the EDC dehydrochlorination to produce VCM. By combining CeO_2 for its high activity towards EDC with Eu_2O_3 or EuOCl for VCM, in the form of homogeneously mixed oxides or as a dual-bed system, respectively, we demonstrated industrially attractive VCM yields (*ca*. 30%). The intensification feasibility studied herein can be anticipated to be more economical than the current two-step process as it enables reduction of the unit operations eliminating the need for the intermediate EDC purification and subsequent cracking steps.

Acknowledgements. This work was sponsored by Swiss National Science Foundation (project no. 200021-156107). The authors acknowledge Dr. R. Hauert (Empa, Switzerland) for XPS analysis.

Supplementary Material. Supplementary information associated with this article, containing additional characterization data, can be found in the online version.

References

[1] Renolit, Everything about PVC, 2015, http://www.renolit.com/fileadmin/renolit/corporate/images/Everything_about_PVC.pdf (accessed July 22, 2016).

[2] Plastics Today, Global PVC demand to grow 3.2% annually through 2021, 2014, http://www.plasticstoday.com/study-global-pvc-demand-grow-32-annually-through-2021/196257501821043 (accessed July 22, 2016).

[3] K. Weissermel, H.-J. Arpe, in: Industrial Organic Chemistry, Wiley-VCH, Weinheim, 2008, pp. 217-224.

[4] E.-L. Dreher, K.K. Beutel, J.D. Myers, T. Lübbe, S. Krieger, L.H. Pottenger, in: Ullmann's Encyclopedia of Industrial Chemistry, Wiley-VCH, Weinheim, 2000, pp. 9-17.

[5] J.S. Naworski, E.S. Velez, in: Applied Industrial Catalysis, Academic Press, New York, 1983, p. 239.

[6] N.B. Muddada, U. Olsbye, L. Caccialupi, F. Cavani, G. Leofanti, D. Gianolio, S. Bordiga, C. Lamberti, Influence of additives in defining the active phase of the ethylene oxychlorination catalyst, Phys. Chem. Chem. Phys. 12 (2010) 5605-5618.

[7] N.B. Muddada, T. Fuglerud, C. Lamberti, U. Olsbye, Tuning the activity and selectivity of $CuCl_2/\gamma$-Al_2O_3 ethene oxychlorination catalyst by selective promotion, Top. Catal. 57 (2014) 741-756.

[8] F.E. Van Rooijen, A. De Bruijn, J. Johan, Catalytic Oxychlorination, US Patent US2009/0054708 A1 (2009), to Albemarle Netherlands B.V.

[9] M. Malentacchi, C. Rubini, Oxychlorination catalytic composition for controlling exothermic reactions in a fixed bed, European Patent 1 020 222 B1 (2004), to Süd Chemie Mt S.R.L.

[10] I.M. Clegg, R. Hardman, Vinyl chloride production process, US Patent 5 728 905 (1998), to EVC Technologies AG.

[11] L.J. Croce, L. Bajars, M. Gabliks, Oxychlorination of hydrocarbons in the presence of non-halide copper containing catalysts, US Patent 4 025 461 (1977), to Petro-Tex Chemical Corporation.

[12] M.E. Jones, M.M. Olken, D.A. Hickman, Process for the conversion of ethylene to vinyl chloride and novel catalyst compositions useful for such process, US Patent 6 909 024 B1 (2005), to The Dow Chemical Company.

[13] M. Scharfe, P.A. Lira-Parada, V. Paunović, M. Moser, A.P. Amrute, J. Pérez-Ramírez, Oxychlorination-dehydrochlorination chemistry on bifunctional ceria catalysts for intensified vinyl chloride production, Angew. Chem. Int. Ed. 55 (2016) 3068-3072.

[14] M.A. Centeno, P. Malet, I. Carrizosa, J.A. Odriozola, Lanthanide doped V_2O_5/Al_2O_3 catalysts: Structure-activity relationship in the SCR of NO_x, J. Phys. Chem. B 104 (2000) 3310-3319.

[15] W.Y. Hernández, F. Romero-Sarria, M.A. Centeno, J.A. Odriozola, *In situ* characterization of the dynamic gold-support interaction over ceria modified Eu^{3+}. Influence of the oxygen vacancies on the CO oxidation reaction, J. Phys. Chem. C 114 (2010) 10857-10865.

[16] T. Montini, M. Melchionna, M. Monai, P. Fornasiero, Fundamentals and catalytic applications of CeO_2-based materials, Chem. Rev. 116 (2016) 5987-6041.

[17] M. Cargnello, N.L. Wieder, T. Montini, R.J. Gorte, P. Fornasiero, Synthesis of dispersible $Pd@CeO_2$ core-shell nanostructures by self-assembly, J. Am. Chem. Soc. 132 (2010) 1402-1409.

[18] K. Tamm, R. Küngas, R.J. Gorte, E. Lust, Solid oxide fuel cell anodes prepared by infiltration of strontium doped lanthanum vanadate into doped ceria electrolyte, Electrochim. Act. 106 (2013) 398-405.

[19] J. Kašpar, P. Fornasiero, M. Graziani, Use of CeO_2-based oxides in the three-way catalysis, Catal. Today 50 (1999) 285-298.

[20] D. Valechha, S. Lokhande, M. Klementova, J. Subrt, S. Rayalu, N.L. Labhsetwar, Study of nano-structured ceria for catalytic CO oxidation, Mater. Chem. 21 (2011) 3718-3725.

[21] C. de Leitenburg, A. Trovarelli, J. Llorca, F. Cavani, G. Bini, The effect of doping CeO_2 with zirconium in the oxidation of isobutene, Appl. Catal. A 139 (1996) 161-173.

[22] A.P. Amrute, C. Mondelli, M. Moser, G. Novell-Leruth, N. López, D. Rosenthal, R. Farra, M.E. Schuster, D. Teschner, T. Schmidt, J. Pérez-Ramírez, Performance, structure, and mechanism of CeO_2 in HCl oxidation to Cl_2, J. Catal. 286 (2012) 287-297.

[23] M. Moser, A.P. Amrute, J. Pérez-Ramírez, Impact of feed impurities on catalysts for chlorine recycling, Appl. Catal. B 162 (2015) 602-609.

[24] J.H. Lunsford, The catalytic oxidative coupling of methane, Angew. Chem. Int. Ed. 34 (1995) 970-980.

[25] T.J. Toops, A.B. Walters, M.A. Vannice, The effect of CO_2 and H_2O on the kinetics of NO reduction by CH_4 over a La_2O_3/γ-Al_2O_3 catalyst, J. Catal. 214 (2003) 292-307.

[26] S.G. Podkolzin, E.E. Stangland, M.E. Jones, E. Peringer, J.A. Lercher, Methyl chloride production from methane over lanthanum-based catalysts, J. Am. Chem. Soc. 129 (2007) 2569-2576.

[27] J. He, T. Xu, Z. Wang, Q. Zhang, W. Deng, Y. Wang, Transformation of methane to propylene: A two-step reaction route catalyzed by modified CeO_2 nanocrystals and zeolites, Angew. Chem. Int. Ed. 51 (2012) 2438-2442.

[28] S. Brunauer, P.H. Emmett, E. Teller, Adsorption of gases in multimolecular layers, J. Am. Chem. Soc. 60 (1938) 309-319.

[29] F. Mercier, C. Alliot, L. Bion, N. Thromat, P. Toulhoat, XPS study of Eu(III) coordination compounds: Core levels binding energies in solid mixed-oxo-compounds $Eu_mX_xO_y$, J. Electron. Spectros. Relat: Phenomena 150 (2006) 21-26.

[30] S. Kumar, R. Prakash, R.J. Choudhary, D.M. Phase, Structural, XPS and magnetic studies of pulsed laser deposited Fe doped Eu_2O_3 thin film, Mater. Res. Bull. 70 (2015) 392-396.

[31] Y. Uwamino, A. Tsuge, T. Ishizuka, H. Yamatera, X-Ray photoelectron spectroscopy of rare earth halides, Bull. Chem. Soc. Jpn. 59 (1986) 2263-2267.

[32] A.S. Shalygin, L.V. Malysheva, E.A. Paukshtis, Mechanism of 1,2-dichloroethane dehydrochlorination on the acid sites of oxide catalysts as studied by IR spectroscopy, Kinet. Catal. 52 (2011) 305-315.

[33] H.C. Yao, Y.F. Yu Yao, Ceria in automotive exhaust catalysts: I. Oxygen storage, J. Catal. 86 (1984) 254-265.

[34] A. Trovarelli, Catalytic properties of ceria and CeO_2-containing materials, Catal. Rev. - Sci. Eng. 38 (1996) 439-518.

[35] R. Farra, S. Wrabetz, M.E. Schuster, E. Stotz, N.G. Hamilton, A.P. Amrute, J. Pérez-Ramírez, N. López, D. Teschner, Understanding CeO_2 as a deacon catalyst by probe molecule adsorption and *in situ* infrared characterizations, Phys. Chem. Chem. Phys. 15 (2013) 3454-3465.

Table 1. Total surface area of the samples prior to (fresh) and after (equilibrated) ethylene oxychlorination. The nomenclature of the used samples reflects the main crystallographic phase identified in the catalyst.

Fresh sample[a]	S_{BET}[b] ($m^2\ g^{-1}$)	**Equilibrated sample**	S_{BET}[b] ($m^2\ g^{-1}$)
La_2O_3	6	$LaCl_3$	8
CeO_2	45	CeO_2	28
Pr_4O_7	5	PrOCl	6
Nd_2O_3	32	$NdCl_3$	21
Sm_2O_3	10	SmOCl	8
Eu_2O_3	11	EuOCl	8
Eu_2O_3-p-773	37	EuOCl-p-773	26
Eu_2O_3-p-973	31	EuOCl-p-973	23
Eu_2O_3-p-1173	14	EuOCl-p-1173	12
Gd_2O_3	5	GdOCl	16
Tb_2O_3	4	TbOCl	7
Dy_2O_3	29	DyOCl	25
Ho_2O_3	7	HoOCl	6
Er_2O_3	60	$ErCl_3$	15

[a] All samples were commercial, except Eu_2O_3-p-T_{cal}, which was obtained by precipitation and calcination at T_{cal} K. [b] BET method.

Table 2. Characterization data and rate of VCM formation of the mixed europium-cerium oxides.

Sample	Eu:Ce[a] (mol mol^{-1})	S_{BET}[b] (m^2 g^{-1})	r(VCM)[c] (mol h^{-1} m^{-2})
Eu_2O_3-p-973	1:0	31	8.96 x 10^{-6}
$Eu_{0.9}Ce_{0.1}O_{1.55}$-cp-773	0.9:0.1	16	9.25 x 10^{-6}
$Eu_{0.5}Ce_{0.5}O_{1.75}$-cp-773	0.51:0.49	13	2.24 x 10^{-5}
$Eu_{0.4}Ce_{0.6}O_{1.8}$-cp-773	0.39:0.61	27	2.36 x 10^{-5}
$Eu_{0.3}Ce_{0.7}O_{1.85}$-cp-773	0.3:0.7	25	1.07 x 10^{-5}
CeO_2-p-773	0:1	44	1.41 x 10^{-5}
CeO_2-p-EuOCl-p-db	0.4:0.6[d]	39[d]	2.49 x 10^{-5}

[a] XRF. [b] BET method. [c] Corresponds to data in **Fig. 8**. [d] Estimated.

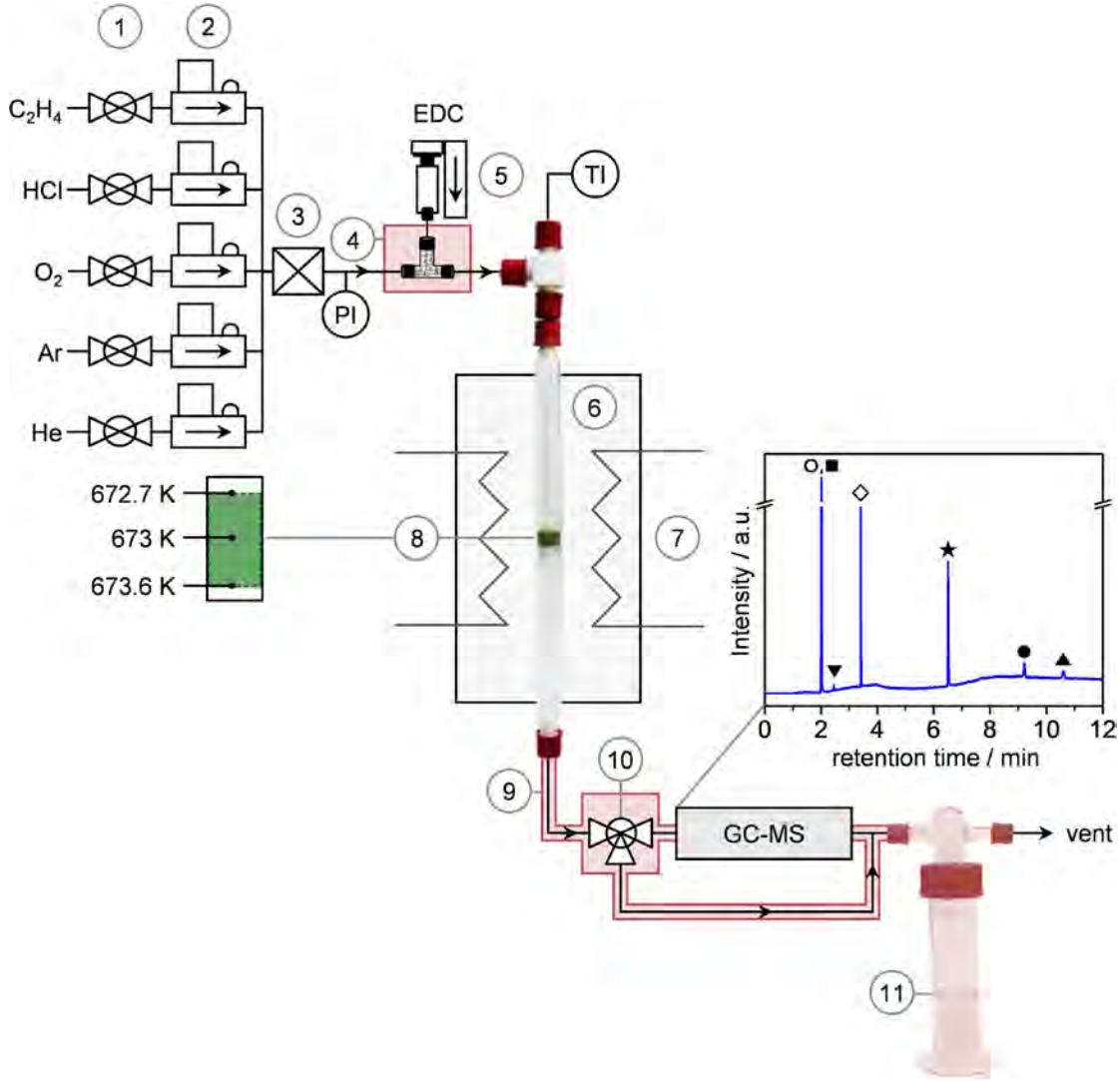

Scheme 1. Scheme of the laboratory set-up used for the catalytic studies. 1: on-off valves, 2: mass flow controllers, 3: mixer, 4: vaporizer, 5: syringe pump, 6: quartz reactor, 7: oven, 8: catalyst bed, 9: heat tracing, 10: three-way bypass valve, 11: NaOH scrubber, PI: pressure indicator, and TI: temperature indicator. The three positions at which the temperature was measured in the catalyst bed are indicated on the left, lying within ±1 K (measured in a reference experiment over CeO_2-1173 at 31% C_2H_4 conversion). The inset on the right depicts a representative chromatogram where the peaks are assigned to the following compounds: ○,■ Ar and CO (due to the overlapping retention time, these peaks were subsequently separated by mass spectrometry), ◇ C_2H_4, ▼ CO_2, ★ vinyl chloride, ● 1,2-cis-dichloroethene, and ▲ ethylene dichloride.

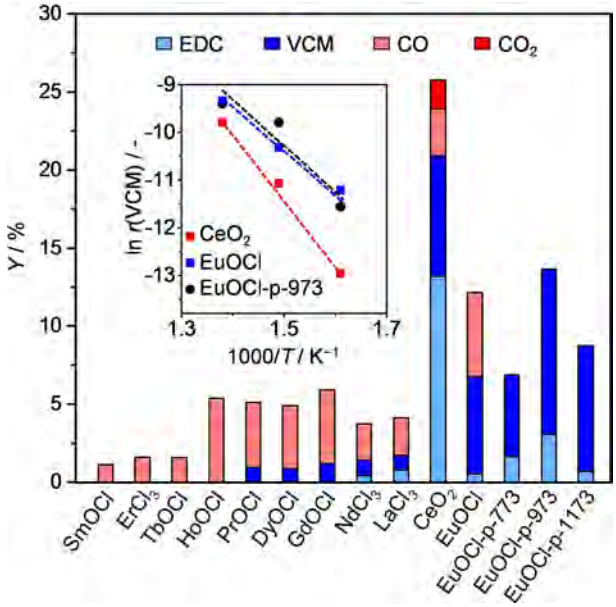

Fig. 1. Product yields (*Y*) in ethylene oxychlorination over single metal lanthanide catalysts. The inset depicts the Arrhenius plot of VCM formation over CeO_2, EuOCl, and EuOCl-p-973. Conditions: T = 723 K, C_2H_4:HCl:O_2:Ar:He = 3:4.8:3:3:86.2, $W_{cat}/\dot{n}^0(C_2H_4)$ = 63 g h mol^{-1}.

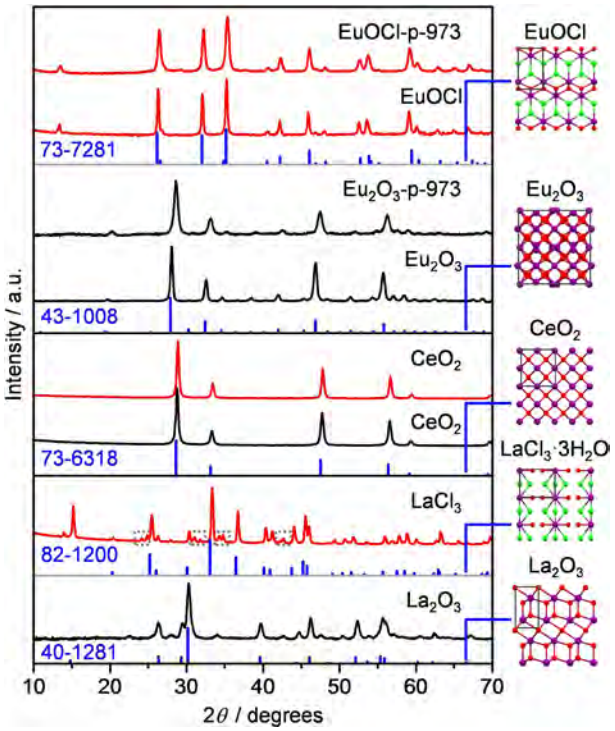

Fig. 2. XRD patterns of selected catalysts prior to (black) and after (red) ethylene oxychlorination. Vertical lines beneath the diffractograms and structures on the right denote identified crystalline phases according to the ICDD PDF numbers provided on the left of the figure. The gray rectangles in the structures represent the corresponding unit cells. Dashed boxes in the diffractogram of $LaCl_3$ highlight the reflections for $LaOCl{\cdot}H_2O$ (ICDD PDF 70-2139). XRD analysis of all other investigated lanthanide-based catalysts is depicted in **Fig. S2**.

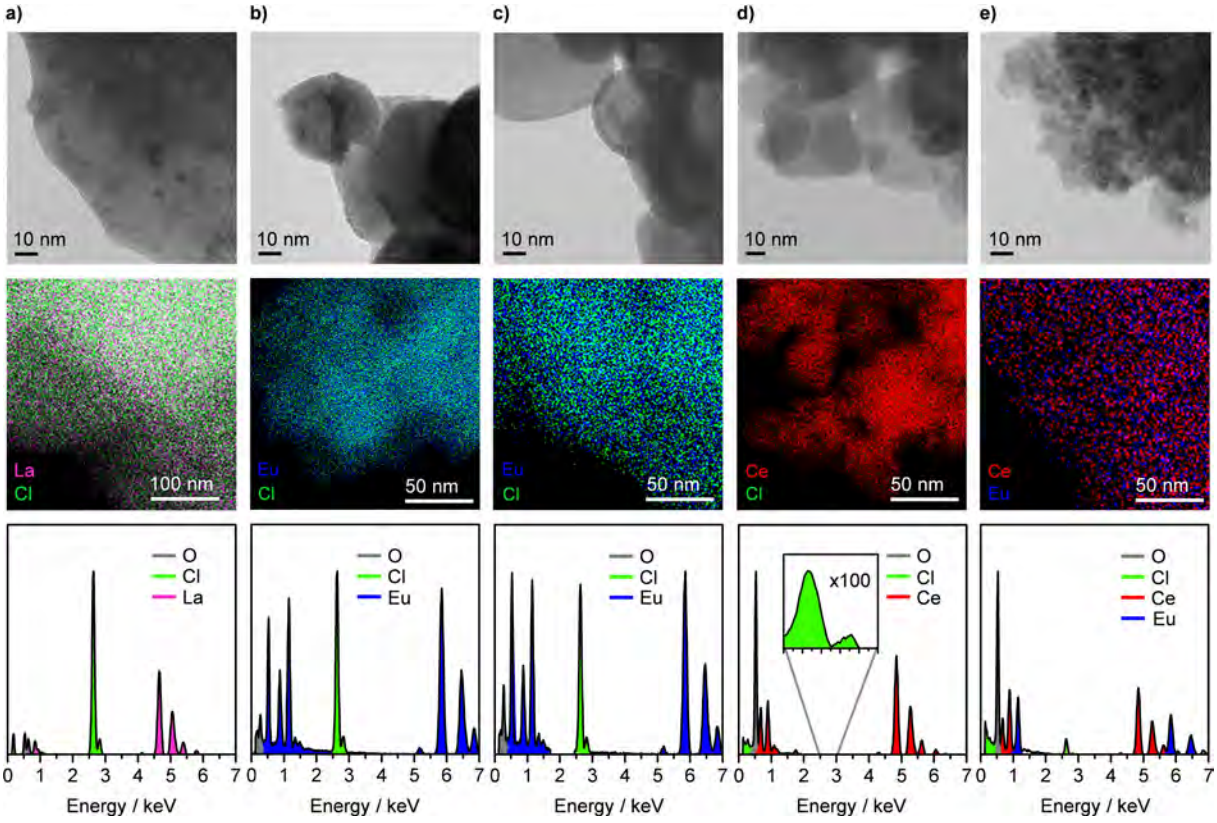

Fig. 3. HRTEM images (top), elemental maps (middle), and corresponding EDX spectra (bottom) of equilibrated catalysts: column **a**) LaOCl, column **b**) EuOCl, column **c**) EuOCl-p-973, column **d**) CeO_2, and column **e**) $Eu_{0.4}Ce_{0.6}O_{1.8}$-cp-773.

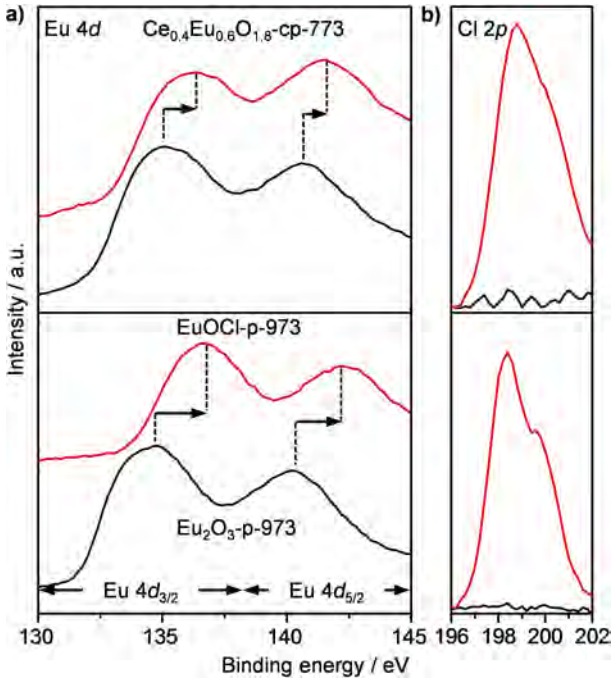

Fig. 4. a) Eu 4*d* and **b**) Cl 2*p* core level XPS spectra of fresh (black) and equilibrated (red) europium-based catalysts.

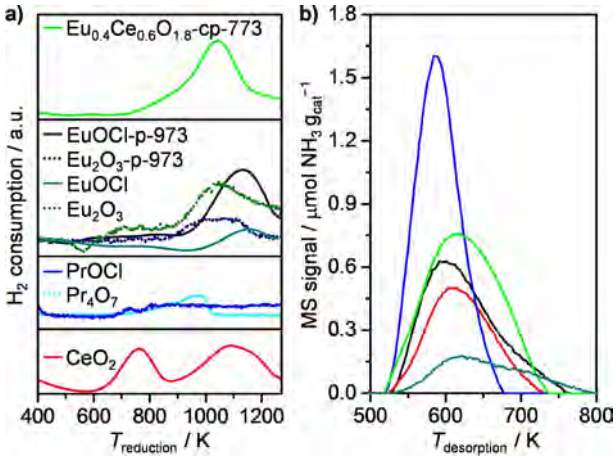

Fig. 5. a) H_2-TPR and **b**) NH_3-TPD profiles of selected fresh (dashed lines) and equilibrated (solid lines) catalysts.

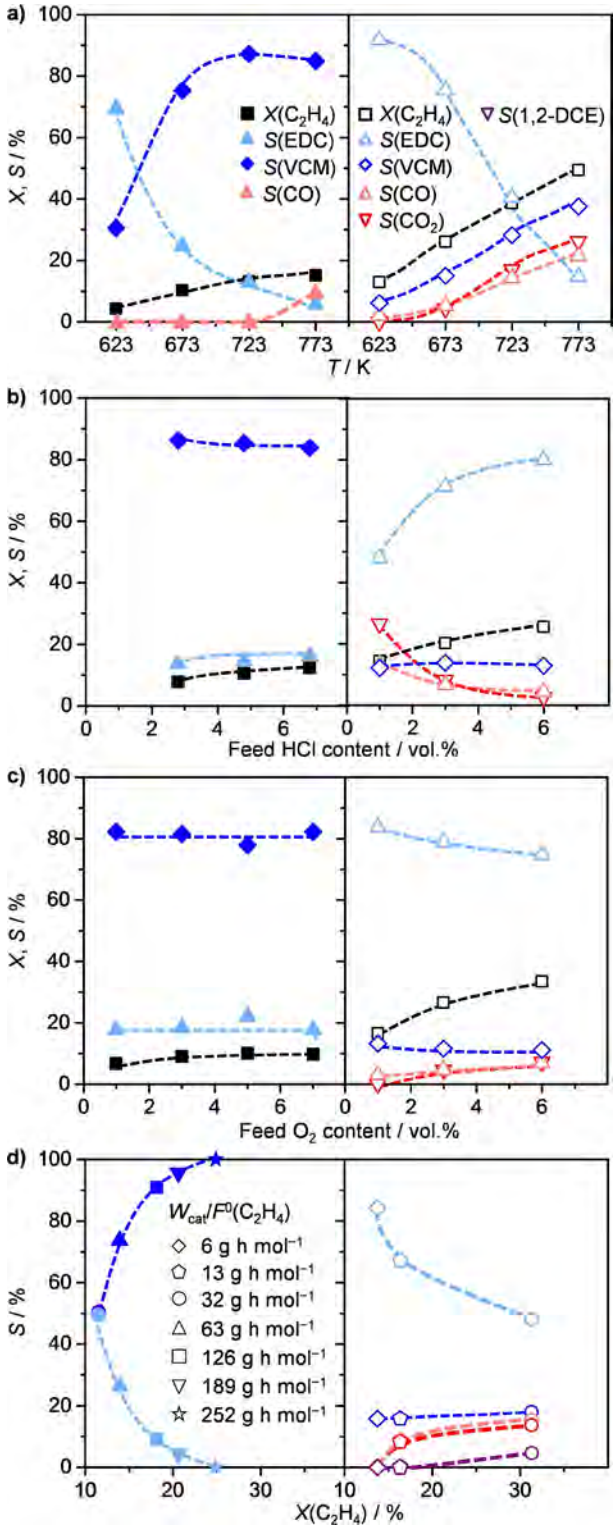

Fig. 6. C_2H_4 conversion and product selectivity over EuOCl-p-973 (left) and CeO_2-1173 (right) as a function of **a**) *T* at fixed HCl (4.8 vol.%) and O_2 (3 vol.%) concentrations, **b**) feed HCl content at fixed O_2 content (3 vol.%) at 723 K (EuOCl) and 673 K (CeO_2), and **c**) feed O_2 content at fixed HCl content (4.8 vol.%) at 723 K (EuOCl) and 673 K (CeO_2). **d**) Selectivity to

products *versus* conversion at different space times at 723 K at fixed HCl (4.8 vol.%) and O_2 (3 vol.%) concentrations, color code as in **a**-**c**. Conditions: **a**-**c**) $W_{cat}/\dot{n}^0(C_2H_4)$ = 63 g h mol^{-1}, **d**) $W_{cat}/\dot{n}^0(C_2H_4)$ = 6-252 g h mol^{-1}.

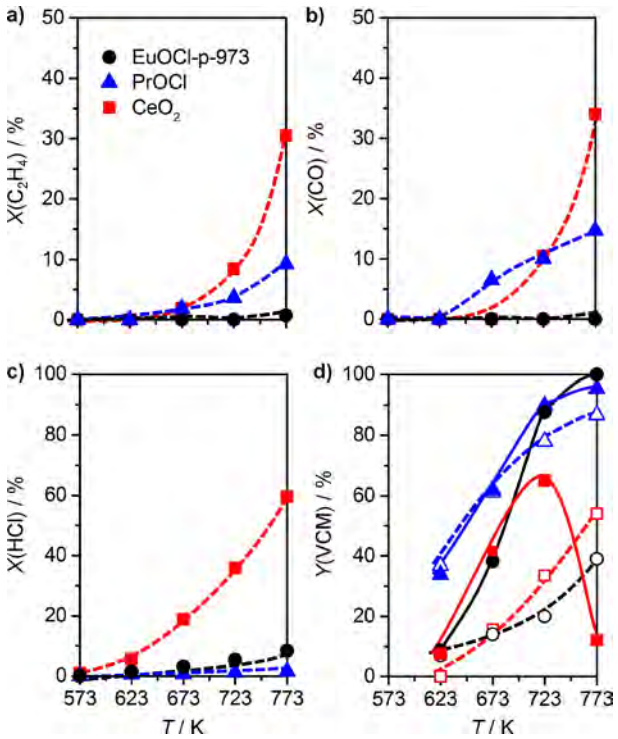

Fig. 7. Performance descriptors for selective VCM production over equilibrated catalysts. **a**) C_2H_4 oxidation to CO_2 (C_2H_4:O_2:Ar:He = 3:3:3:91, $W_{cat}/\dot{n}^0(C_2H_4)$ = 63 g h mol^{-1}), **b**) CO oxidation to CO_2 (CO:O_2:Ar:He = 2.5:2.5:3:92, $W_{cat}/\dot{n}^0$(CO) = 76 g h mol^{-1}), **c**) HCl oxidation to Cl_2 (HCl:O_2:Ar:He = 3:3:3:91, $W_{cat}/\dot{n}^0$(HCl) = 63 g h mol^{-1}), and **d**) EDC dehydrochlorination to VCM. In **d**) $W_{cat}/\dot{n}^0$(EDC) = 126 g h mol^{-1}, open symbols: EDC:Ar:He = 1.5:3:95.5, and solid symbols: EDC:HCl:O_2:Ar:He = 1.5:4.8:3:3:87.7.

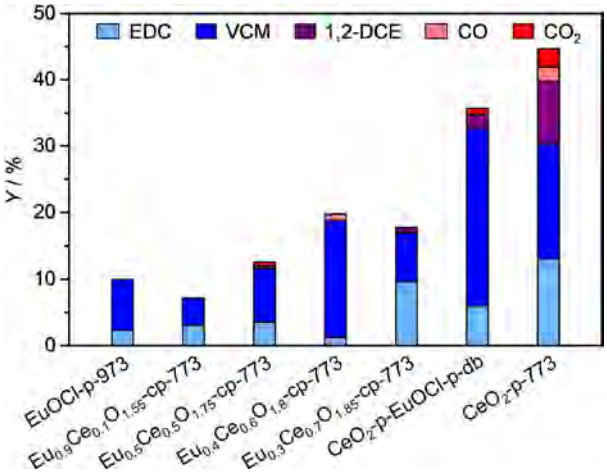

Fig. 8. Product yields in ethylene oxychlorination over EuOCl-p-973, CeO_2-p-773, mixed oxides of Eu and Ce, and the dual-bed configuration of CeO_2-p-773 and EuOCl-p-973. Conditions: T = 673 K, C_2H_4:HCl:O_2:Ar:He = 3:4.8:3:3:86.2, $W_{cat}/\dot{n}^0(C_2H_4)$ = 63 g h mol^{-1}.

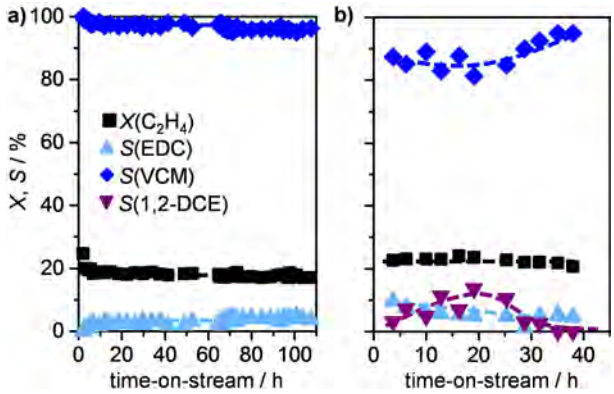

Fig. 9. C_2H_4 conversion and product selectivities *versus* time-on-stream in ethylene oxychlorination over **a**) EuOCl-p-973 and **b**) $Eu_{0.4}Ce_{0.6}O_{1.8}$-cp-773. Conditions: T = 723 K (673 K for $Eu_{0.4}Ce_{0.6}O_{1.8}$-cp-773), C_2H_4:HCl:O_2:Ar:He = 3:4.8:1.5:3:87.7 (C_2H_4:HCl:O_2:Ar:He = 3:4.8:3:3:86.2 for $Eu_{0.4}Ce_{0.6}O_{1.8}$-cp-773), $W_{cat}/\dot{n}^0(C_2H_4)$ = 252 g h mol^{-1} (63 g h mol^{-1} for $Eu_{0.4}Ce_{0.6}O_{1.8}$-cp-773).

Supplementary Material

Lanthanide compounds as catalysts for the one-step synthesis of vinyl chloride from ethylene

Matthias Scharfe,[†] Pedro A. Lira-Parada,[†] Amol P. Amrute, Sharon Mitchell, and Javier Pérez-Ramírez*

Institute for Chemical and Bioengineering, Department of Chemistry and Applied Biosciences,
ETH Zurich, Vladimir-Prelog-Weg 1, 8093 Zurich, Switzerland.

[†] Equal contribution | * Corresponding author. E-mail: jpr@chem.ethz.ch.

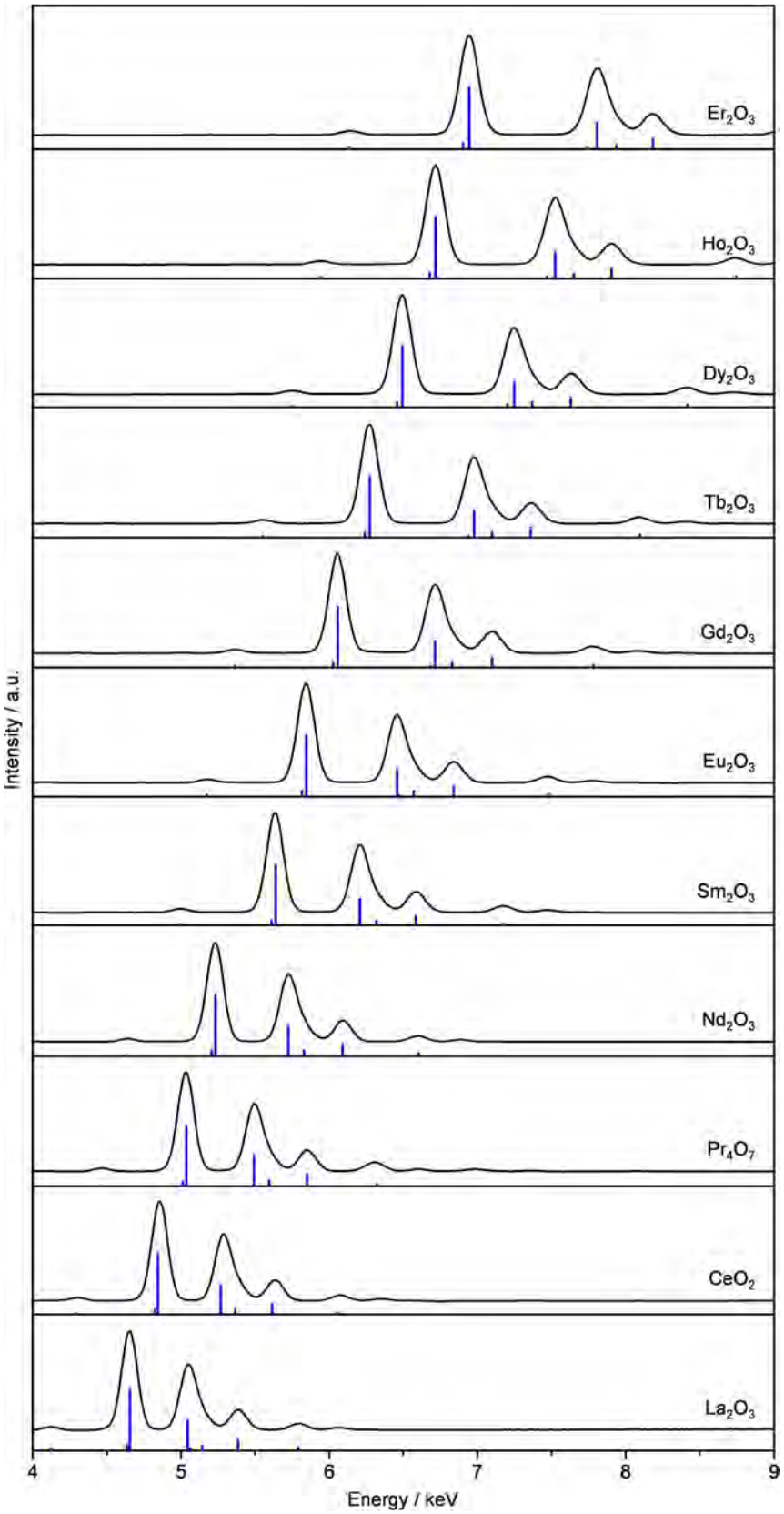

Fig. S1. X-ray fluorescence spectra of commercial lanthanide oxides. Vertical lines show the reference positions of the respective lanthanide. The excellent match of the reference line with the measured spectra confirms the high purity of the samples.

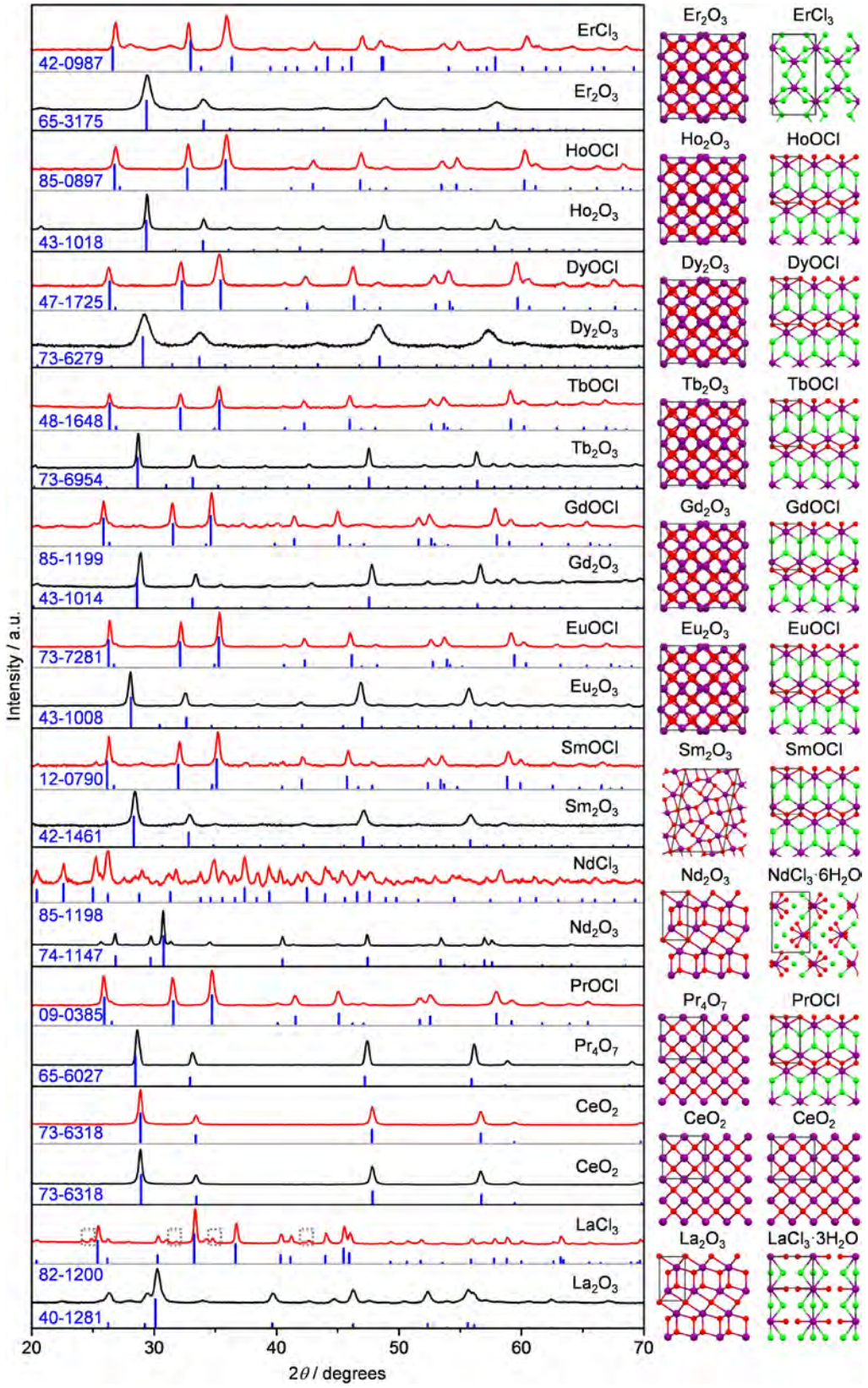

Fig. S2. X-ray diffraction patterns of the samples prior to (black) and after (red) the oxychlorination of ethylene. Vertical lines beneath the diffractograms and structures on the right denote identified crystalline phases according to the ICDD PDF numbers provided on the left of the figure. The gray rectangles in the structures represent the

corresponding unit cells. Dashed boxes in the diffractogram of $LaCl_3$ indicate the reflections for $LaOCl{\cdot}H_2O$ (ICDD PDF 70-2139). All oxides matched the supplier specification except Pr_2O_3, which showed the reflections of Pr_4O_7.

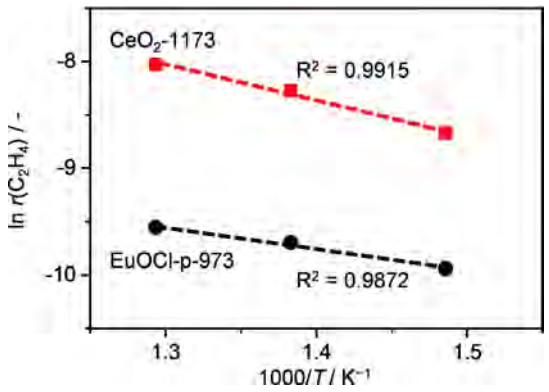

Fig. S3. The Arrhenius plot of C_2H_4 conversion in ethylene oxychlorination over EuOCl-p-973 and CeO_2-1173. Conditions: C_2H_4:HCl:O_2:Ar:He = 3:4.8:3:3:86.2, $W_{cat}/\dot{n}^0(C_2H_4)$ = 63 g h mol^{-1}.

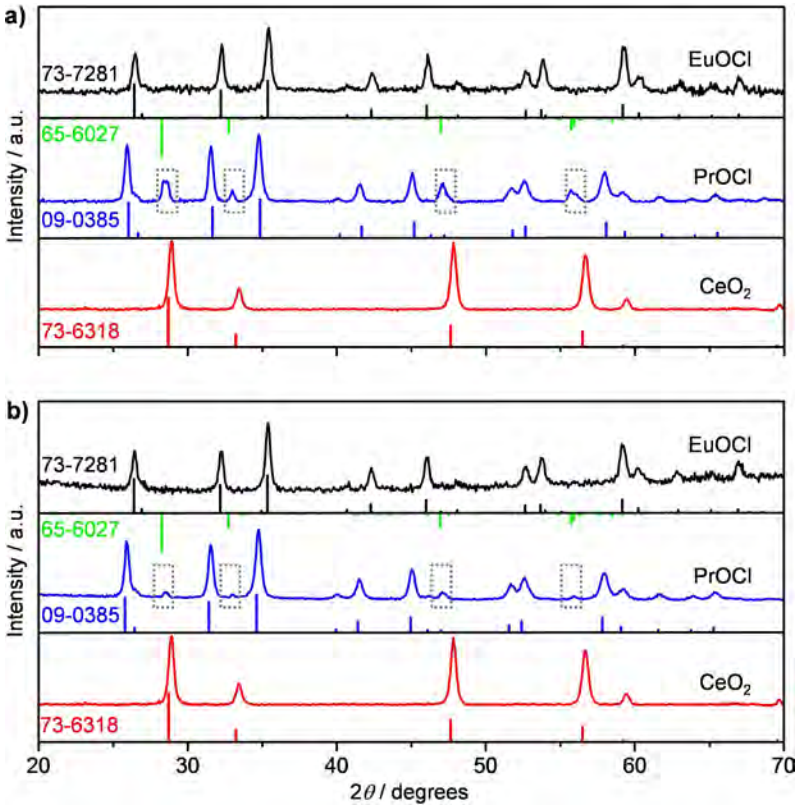

Fig. S4. X-ray diffraction patterns of EuOCl, PrOCl, and CeO_2 **a**) after C_2H_4 oxidation and **b**) after CO oxidation. Vertical lines show the phases identified in the samples: red (CeO_2), green (Pr_4O_7), blue (PrOCl), and black (EuOCl). ICDD PDF numbers are provided on the left of the figure. Dashed boxes in PrOCl diffractograms show the Pr_4O_7 phase that is formed from PrOCl upon oxidation of C_2H_4/CO.

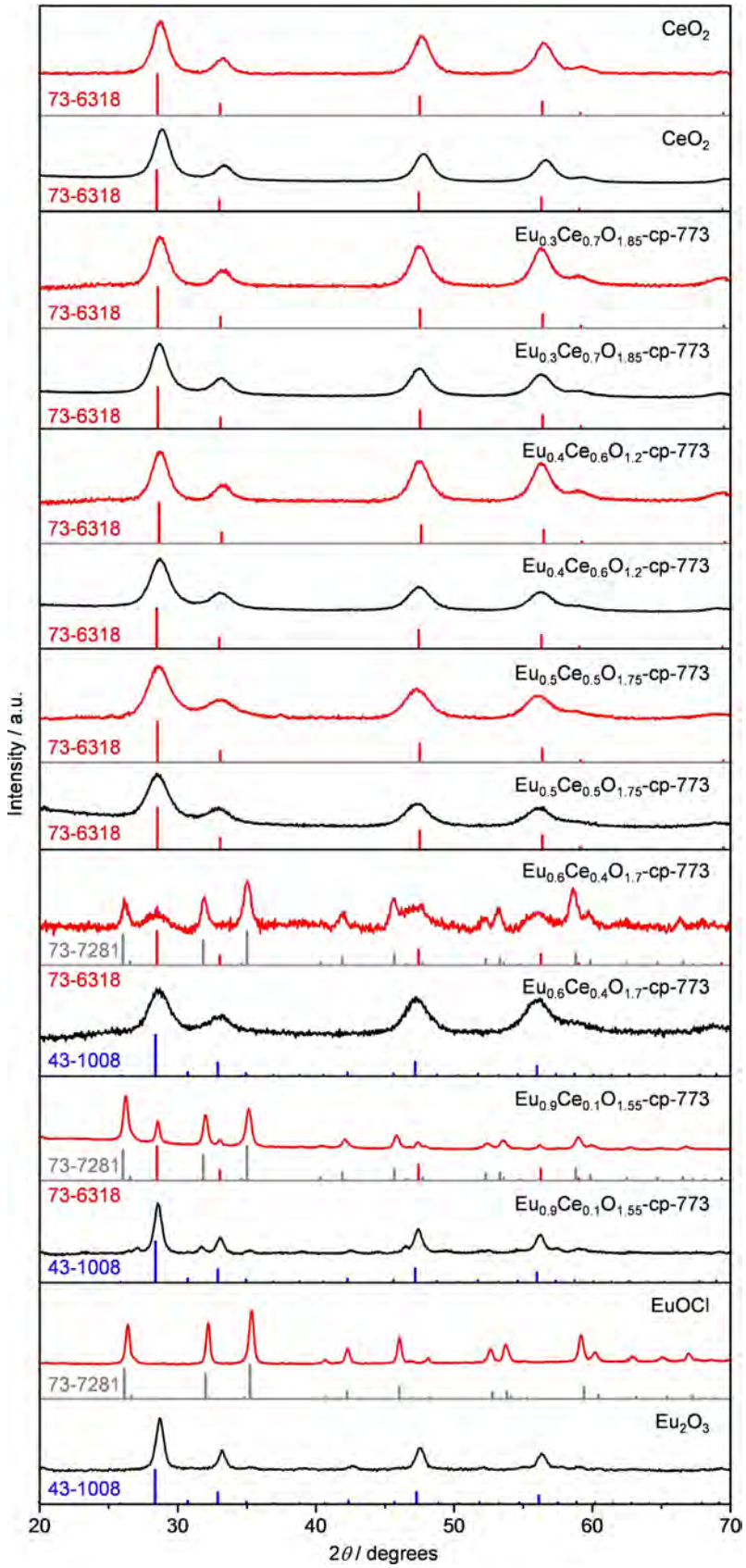

Fig. S5. X-ray diffraction patterns of mixed europium-cerium oxides prior to (black) and after (red) the oxychlorination of ethylene. Vertical lines denote the crystalline phases identified in the solids: red (CeO_2), gray (EuOCl), and blue (Eu_2O_3). ICDD PDF numbers are provided on the left of the figure.